Molecular Receptors for Adenine and Guanine Employing Metal Coordination, Hydrogen-Bonding and π-Stacking Interactions

James E. Kickham, Stephen J. Loeb* and Shannon L. Murphy

Abstract: Thiacyclophane ligands **1** and **2**, containing a *meta*-xylyldithiaether unit, an aromatic spacing unit and a polyether chain, were prepared in good yield in a three-step synthesis. The macrocyclic organopalladium complexes [Pd(L)(MeCN)][BF_4] (**3**: L = 1; **4**: L = **2**) were prepared through palladation of the respective thiacyclophane ligand by reaction with [$Pd(MeCN)_4$][BF_4]$_2$. These complexes act as *metalloreceptors* to aromatic amines such as *p*-aminopyridine (pap), *m*-aminopyridine (map) and the DNA nucleobases adenine and guanine. Binding occurs through simultaneous first- and second-sphere coordination. This involves three separate interactions: first-sphere σ donation from an aromatic N atom to the Pd centre, second-sphere hydrogen bonds between the NH_2 group and polyether O atoms, and π stacking between the electron-poor aromatic rings of the substrate and the electron-rich aromatic spacing units of the receptor. ^{1}H NMR spectra exhibit chemical shift changes indicative of the H-bonding and π-stacking interactions in solution. X-ray structures for thiacyclophane **1**, metalloreceptor [Pd(**1**)(MeCN)][BF_4] (**3**), metalloreceptor/model substrate complexes [Pd(**1**)(pap)][BF_4] (**5**) and [Pd(**2**)(pap)][BF_4] (**7**), and metalloreceptor/nucleobase complexes [Pd(**1**)(adenine)][BF_4] (**13**), [Pd(**2**)(adenine)][BF_4] (**14**) and [Pd(**1**)(guanine-BF_3)][BF_4] (**15b**) show details of these interactions in the solid state.

Keywords
hydrogen bonds · metalloreceptor · molecular recognition · nucleobases · pi interactions

Introduction

A substrate molecule may interact with a transition metal containing receptor such that it occupies sites in both the first and second coordination spheres. This phenomenon is known as *simultaneous* first- and second-sphere coordination.[1] We have recently reported that organopalladium crown ether complexes can act as metalloreceptors through σ donation to the transition metal (Pd) and hydrogen bonding to peripheral ether oxygen sites on the ligand (Scheme 1).[2] This type of multiple-point binding has been applied to the molecular recognition of DNA nucleobases cytosine[3] and thymine,[4] barbiturates,[5e] and amino acids[6] as well as to the design of receptors for binding amines and the hydrazinium ion.[2]

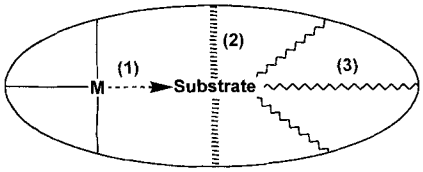

Scheme 1. Schematic representation of a metalloreceptor capable of binding a substrate molecule by employing a combination of 1) metal coordination, 2) π stacking and 3) hydrogen bonding.

Most metalloreceptors reported to date employ hydrogen bonding as the primary noncovalent, second-sphere interaction to bind a substrate.[2-6] There is, however, a great deal of research into the design and synthesis of organic hosts that employ π-stacking interactions (Scheme 1),[7] since this type of charge-transfer interaction has been identified as occurring between DNA base pairs in the double helix.[8]

In a previous communication, it was demonstrated that palladium metalloreceptors based on thiacyclophane ligands **1** and **2** (Scheme 2) were selective for the purine nucleobases adenine and guanine over the pyrimidine nucleobases cytosine and thymine.[3] These preliminary binding studies suggested that the organopalladium complexes act as metalloreceptors by employ-

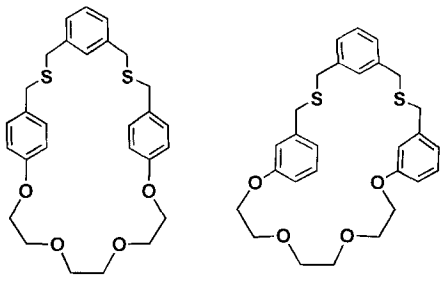

1 2

Scheme 2. Thiacyclophanes **1** and **2** with *para*- and *meta*-substituted aromatic spacing units, respectively, and crown ether binding sites.

[*] S. J. Loeb, J. E. Kickham, S. L. Murphy
Department of Chemistry and Biochemistry, University of Windsor
Windsor, Ontario, N9B 3P4 (Canada)
Fax: Int code +(519)973-7098
e-mail: loeb@uwindsor.ca

ing *three* different types of bonding interactions: σ donation to the palladium centre, π stacking of the substrate with the aromatic units of the receptor and hydrogen bonding to the peripheral ether oxygen sites (Scheme 1). In this article, we report the syntheses of these macrocyclic metalloreceptors along with the detailed solution and solid state investigations of their binding properties.

Results and Discussion

Synthesis and Characterization of 1 and 2: Thiacyclophanes **1** and **2** were prepared by a straightforward, three-step process employing commercially available starting materials as outlined in Scheme 3 for **1**. The ring closure step involved the reaction between dithiol and dichloride by Kellogg's Cs^+-mediated method in DMF solution.[9] This synthetic route produced **1** and **2** as colourless, crystalline materials in moderate overall yields of 20 and 34% based on the starting hydroxybenzyl alcohol.

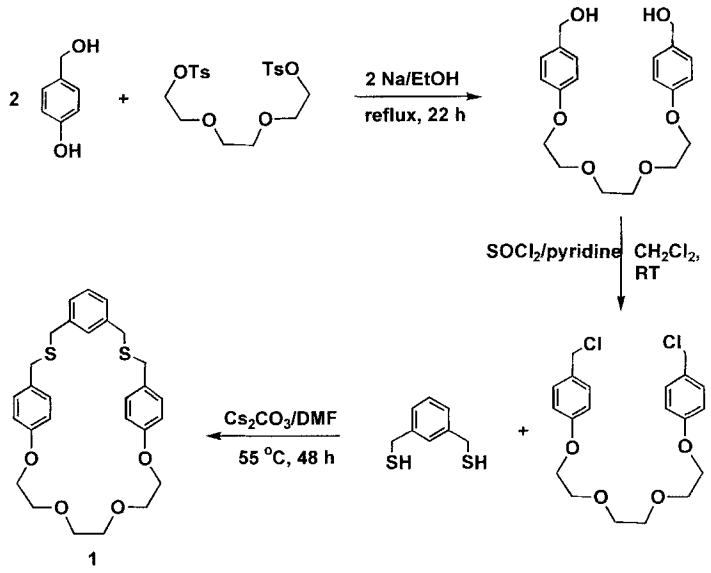

Scheme 3. Outline of the synthetic route to thiacyclophane **1**.

The ^{1}H NMR spectrum of **1** contains well-separated resonances attributable to three sets of OCH_2 protons, two types of benzylic protons and two distinguishable sets of aromatic protons due to the 1,3-xylyldithioether fragment and the *para*-substituted aromatic spacer group. For **2**, a very similar pattern is observed; however, the two sets of aromatic protons overlap and the benzylic resonances are coincidental. The $^{13}C\{^1H\}$ NMR spectra for these ligands showed well-resolved peaks for all carbon atoms, and full spectral interpretations were relatively straightforward. Ligand **1** was further characterized by a single-crystal X-ray diffraction study (Table 1). A perspective ORTEP drawing of macrocycle **1** is shown in Figure 1, and some relevant bonding parameters are listed in Table 2.

Table 1. Summary of crystallographic data for ligand **1**, metalloreceptor **3** and complexes **5** and **7** with model substrate *p*-aminopyridine (pap).

	1	**3**	**5**	**7**
formula	$C_{23}H_{35}O_4S_2$	$C_{30}H_{44}BF_4NO_4PdS_2$	$C_{33}H_{37}BF_4N_2O_4PdS_2$	$C_{33}H_{37}BF_4N_2O_4PdS_2$
M_r	496.68	729.93	782.99	782.99
a, Å	15.157(4)	12.076(2)	14.329(3)	9.310(5)
b, Å	15.361(6)	12.314(2)	15.123(2)	24.202(5)
c, Å	5.658(2)	11.730(2)	8.832(1)	15.518(4)
α, °	99.96(3)	109.59(1)	99.04(1)	–
β, °	93.20(3)	106.18(1)	97.22(2)	105.93(3)
γ, °	80.53(3)	75.73(1)	114.83(2)	–
space group	$P\bar{1}$ (no. 2)	$P\bar{1}$ (no. 2)	$P\bar{1}$ (no. 2)	$P2_1/n$ (no. 14)
V, Å^3	1279.2(8)	1555.3(4)	1675.8(6)	3362(2)
ρ, g cm^{-3}	1.29	1.56	1.55	1.55
Z	2	2	2	4
μ, cm^{-1}	2.40	7.91	7.41	7.41
λ, Å	0.7017	0.7017	0.7017	0.7017
T, °C	23	23	23	23
goodness of fit	1.59	2.14	1.32	1.62
$R(F_o)$, % [a]	3.45	4.18	3.51	5.19
$R_w(F_o)$, % [b]	4.68	4.51	3.98	5.44

[a] $R = \sum||F_o| - |F_c||/\sum|F_o|$. [b] $R_w = (\sum w(|F_o| - |F_c|)^2/\sum wF_o^2)^{1/2}$ and $w = 1/\sigma^2(F)$.

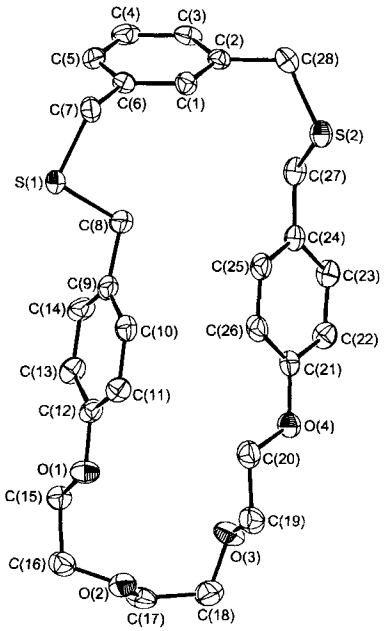

Figure 1. X-ray structure of thiacyclophane **1** showing the atom numbering scheme.

Table 2. Selected bond lengths (Å) and angles (°) for thiacyclophane **1**.

S(1)–C(7)	1.821(4)	S(1)–C(8)	1.796(4)
S(2)–C(27)	1.806(4)	S(2)–C(28)	1.817(4)
O(1)–C(12)	1.375(4)	O(1)–C(15)	1.419(5)
O(2)–C(16)	1.423(5)	O(2)–C(17)	1.417(5)
O(3)–C(18)	1.414(5)	O(3)–C(19)	1.398(5)
O(4)–C(20)	1.438(5)	O(4)–C(21)	1.363(5)
C(2)–C(28)	1.503(5)	C(6)–C(7)	1.497(6)
C(8)–C(9)	1.512(6)	C(15)–C(16)	1.499(6)
C(19)–C(20)	1.491(6)	C(24)–C(27)	1.508(5)
C(7)-S(1)-C(8)	98.4(2)	C(27)-S(2)-C(28)	100.1(2)
C(12)-O(1)-C(15)	118.8(3)	C(16)-O(2)-C(17)	113.6(4)
C(18)-O(3)-C(19)	114.4(4)	C(20)-O(4)-C(21)	117.1(3)
S(1)-C(7)-C(6)	114.6(3)	S(1)-C(8)-C(9)	111.4(3)
C(8)-C(9)-C(10)	121.7(5)	C(8)-C(9)-C(14)	119.7(5)
O(1)-C(12)-C(13)	114.8(4)	O(1)-C(12)-C(11)	125.1(4)
O(1)-C(15)-C(16)	107.0(4)	O(2)-C(16)-C(15)	112.2(4)
O(2)-C(17)-C(18)	109.7(4)	O(3)-C(18)-C(17)	111.0(4)
O(3)-C(19)-C(20)	110.2(4)	O(4)-C(20)-C(19)	108.9(4)
S(2)-C(27)-C(24)	113.2(3)	S(2)-C(28)-C(2)	115.5(3)

0947-6539/97/0308-1204 $ 17.50+.50/0 Chem. Eur. J. 1997, 3, No. 8

Synthesis and Characterization of Metalloreceptors 3 and 4: The palladium centre and ancillary acetonitrile group were incorporated into the macrocycles **1** and **2** through direct metalation of the xylyl aromatic ring by reaction with $[Pd(MeCN)_4][BF_4]_2$ in acetonitrile solution. The complexes **3** and **4** are yellow, air-stable crystalline solids, which are soluble in most polar organic solvents and appear to be air-stable in solution for prolonged periods of time (Scheme 4).

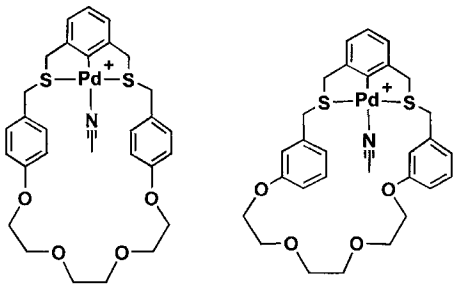

Scheme 4. Metalloreceptors **3** and **4** prepared from thiacyclophanes **1** and **2**. Each contains a Pd^{II} coordination site (with a labile acetonitrile ligand) in addition to the aromatic spacing units and crown ether binding site.

The ^1H NMR spectra indicate that metalation produces chemical shift changes similar to those observed in other metalated thiacyclophanes.[2, 10] In particular, disappearance of the aromatic resonance attributable to the proton at the 2-position of the 1,3-xylyldithioether fragment, and the downfield shift and broadening of the benzylic resonances are diagnostic of palladation. A single broad resonance for the *meta*-xylyl S-benzyl protons indicates that the size of the macrocyclic cavity is such that inversion at sulfur is facile at room temperature.[2, 10] This is in contrast to some previously studied palladated macrocycles of this type in which a smaller polyether ring prevented inversion at sulfur and resulted in an AB pattern for these protons.[2, 10]

Complex **3** was further characterized by a single-crystal X-ray diffraction study. A perspective ORTEP drawing is shown in Figure 2 and some relevant bonding parameters are listed in Table 3. The Pd centre adopts a slightly distorted square-planar geometry in which three of the four coordination sites are occupied by the rigid S_2C chelate of the metalated macrocycle. The fourth coordination site *trans* to the Pd–C bond is occupied by a molecule of acetonitrile. The bound MeCN molecule is oriented into the cavity of the macrocycle between the aromatic spacing units, which are almost perpendicular to each other with a dihedral angle of 83.5°. This demonstrates that a substrate bound in place of the labile solvent would be positioned inside the cavity with potential for noncovalent binding, as designed.

In order to investigate this hypothesis, two separate sets of binding studies were performed with metalloreceptors **3** and **4**. The first involved 1:1 binding of the model substrates *para*- and *meta*-aminopyridine and the second involved interaction with the DNA nucleobases adenine and guanine.

Synthesis and Characterization of Metalloreceptor–Aminopyridine Complexes: Metalloreceptors **3** and **4** were each treated with an equivalent of *para*-aminopyridine (pap) and *meta*-aminopyridine (map) to yield the complexes $[Pd(\mathbf{1})(pap)][BF_4]$ (**5**), $[Pd(\mathbf{1})(map)][BF_4]$ (**6**), $[Pd(\mathbf{2})(pap)][BF_4]$ (**7**) and $[Pd(\mathbf{2})map)][BF_4]$ (**8**) in essentially quantitative yield. The interaction between metalloreceptor and substrate was then studied in solution by ^1H NMR spectroscopy and, where possible, in the solid state by X-ray diffraction.

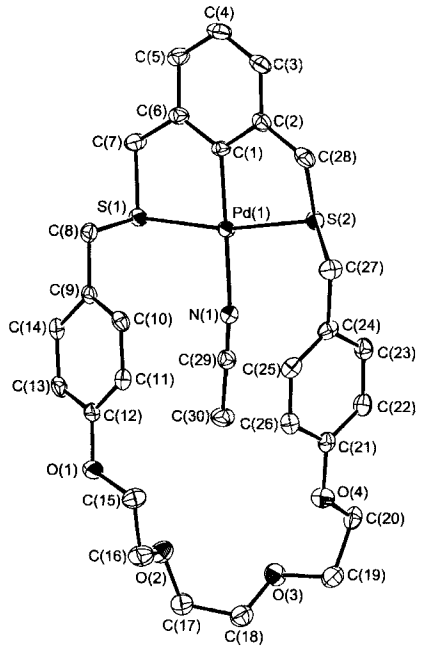

Figure 2. X-ray structure of **3** showing the atom numbering scheme. Metalloreceptor **3** contains three different binding sites for multiple point interaction with a substrate: 1) Pd^{II} coordination site (occupied by a labile acetonitrile ligand) for σ donation, 2) aromatic spacing units for π-stacking interactions and 3) a crown ether binding site for hydrogen bonding.

Table 3. Selected bond lengths (Å) and angles (°) for $[Pd(\mathbf{1})(MeCN)][BF_4]$ (**3**).

Pd(1)–S(1)	2.316(2)	Pd(1)–S(2)	2.310(2)
Pd(1)–N(1)	2.131(5)	Pd(1)–C(1)	1.988(5)
S(1)–C(7)	1.821(6)	S(1)–C(8)	1.828(6)
S(2)–C(27)	1.828(6)	S(2)–C(28)	1.818(6)
O(1)–C(12)	1.373(6)	O(1)–C(15)	1.435(7)
O(2)–C(16)	1.417(8)	O(2)–C(17)	1.418(7)
O(3)–C(18)	1.394(8)	O(3)–C(19)	1.423(8)
O(4)–C(20)	1.431(7)	O(4)–C(21)	1.370(7)
N(1)–C(29)	1.119(7)	C(6)–C(7)	1.503(8)
C(2)–C(28)	1.503(8)	C(29)–C(30)	1.465(8)
C(8)–C(9)	1.496(7)	C(15)–C(16)	1.495(9)
C(17)–C(18)	1.491(9)	C(19)–C(20)	1.498(9)
C(24)–C(27)	1.517(8)		
S(1)-Pd(1)-S(2)	167.68(6)	S(1)-Pd(1)-N(1)	92.3(1)
S(1)-Pd(1)-C(1)	84.9(2)	S(2)-Pd(1)-N(1)	99.2(1)
S(2)-Pd(1)-C(1)	83.4(2)	N(1)-Pd(1)-C(1)	175.6(2)
C(7)-S(1)-C(8)	103.3(3)	C(27)-S(2)-C(28)	99.8(3)
C(12)-O(1)-C(15)	118.9(5)	C(16)-O(2)-C(17)	113.1(5)
C(18)-O(3)-C(19)	114.1(5)	C(20)-O(4)-C(21)	118.2(5)
C(1)-C(2)-C(28)	118.2(5)	C(3)-C(2)-C(28)	121.7(6)
C(1)-C(6)-C(7)	120.3(5)	C(5)-C(6)-C(7)	120.2(6)
S(1)-C(7)-C(6)	110.8(4)	S(1)-C(8)-C(9)	107.4(4)
C(8)-C(9)-C(10)	123.5(6)	C(8)-C(9)-C(14)	119.1(6)
O(1)-C(12)-C(11)	124.1(6)	O(1)-C(12)-C(13)	116.0(6)
O(1)-C(15)-C(16)	109.2(6)	O(2)-C(16)-C(15)	108.3(5)
O(2)-C(17)-C(18)	113.3(6)	O(3)-C(18)-C(17)	108.7(6)
O(3)-C(19)-C(20)	107.7(5)	O(4)-C(20)-C(19)	106.0(5)
O(4)-C(21)-C(22)	125.0(6)	O(4)-C(21)-C(26)	114.8(5)
C(23)-C(24)-C(27)	120.4(6)	C(25)-C(24)-C(27)	120.1(6)
S(2)-C(27)-C(24)	112.5(4)	S(2)-C(28)-C(2)	108.4(4)
N(1)-C(29)-C(30)	179.2(7)		

Table 4 shows a comparison of substrate chemical shifts in the ^{1}H NMR spectra of free *p*-aminopyridine, **5**, **7** and the adduct [Pd(**9**)(pap)][BF_4] (**11**), where **9** is the acyclic dithiaether 1,3-bis(*n*-butylthiomethyl)benzene (Scheme 5). This data is consistent with the occurrence of *three* different types of interaction between the metalloreceptor and substrate: coordination through a first-sphere Pd–N σ bond, second-sphere NH···O hydrogen bonding and π-stacking interactions. There is a slight downfield shift of both the substrate aromatic protons H_α and H_β (ca. 0.1 ppm) and of the substituent NH_2 protons (0.32 ppm) upon coordination of *p*-aminopyridine to Pd in complex **10**. Although somewhat smaller than sometimes observed,[2] these shifts must be due to formation of the first-sphere Pd–N σ bond, since no hydrogen-bonding or π-stacking interactions are possible. For complexes **5** and **7**, in which one or both of the *para*-NH_2 hydrogen atoms could be directed towards the polyether chain of the metalloreceptor, a further downfield shift of 0.25 (**5**) and 0.14 (**7**) ppm is observed for the amino protons. This is attributed to the second-sphere hydrogen-bonding interaction between the substrate amino group and the polyether oxygens of the metalloreceptor. The evidence for π stacking interactions between the electron-poor substrate and the electron-rich aromatic spacing units of the receptor is quite compelling as the aromatic protons H_α and H_β show significant *upfield* shifts ranging from 0.37–1.29 ppm in complexes **5** and **7**. The direction and size of the chemical shift changes are consistent with significant second-sphere charge-transfer interactions occurring between the bound substrate and the aromatic spacing units of the metalloreceptor.

Table 4. ^{1}H NMR spectral evidence of π stacking and hydrogen bonding in metalloreceptor complexes of *p*-aminopyridine (pap).

Complex	H_α [a]	H_β	NH_2
p-aminopyridine (pap)	8.04	6.54	4.82
[Pd(**9**)(pap)][BF_4] (**11**)	8.04	6.64	5.14
[Pd(**1**)(pap)][BF_4] (**5**)	6.75	5.91	5.39
[Pd(**2**)(pap)][BF_4] (**7**)	7.10	6.27	5.28

[a] All chemical shifts are in ppm relative to TMS. H_α and H_β are the protons *ortho* and *meta* to the pyridine nitrogen atom of pap.

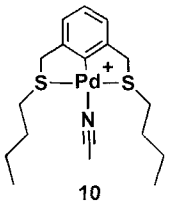

Scheme 5. Complex **10**, prepared by palladation of the acyclic dithiaether **9**, was used specifically for observing coordination of pap and map in the absence of π-stacking or H-bonding interactions.

The X-ray structures of **5** and **7** were determined and provide evidence to support the nature of the metalloreceptor–substrate interactions proposed from NMR spectral data in solution. A perspective ORTEP drawing of **5** is shown in Figure 3 and some relevant bonding parameters are listed in Table 5. The coordination geometry of the $Pd(S_2C)$ unit remains unperturbed by the binding of a substrate, and the bonding parameters associated with the unit are similar to those found for **3**. The receptor binding site *trans* to the Pd–C bond is occupied by the pap substrate, which is coordinated through the aromatic N atom. This arrangement orients the *para*-amino group towards the polyether chain of the receptor, and an intramolecular hydrogen-bonding interaction occurs [H(N2B)···O(3) 2.310(6) Å and N(2)–H(N2B)···O(3) 142.1(4)°]. An intermolecular hydrogen bond also occurs in the solid state between substrate and BF_4^- anion [H(N2A)···F(1) 2.208(4) Å and N(2)–H(N2A)···F(1) 142.3(4)°]. This hydrogen-bonding scheme is accompanied by the π stacking of *one* of the aromatic rings of the metalloreceptor with the aromatic ring of the pap substrate; the dihedral angle is 2.03°.

A perspective ORTEP drawing of **7** is shown in Figure 4, and some relevant bonding parameters are listed in Table 6. Again,

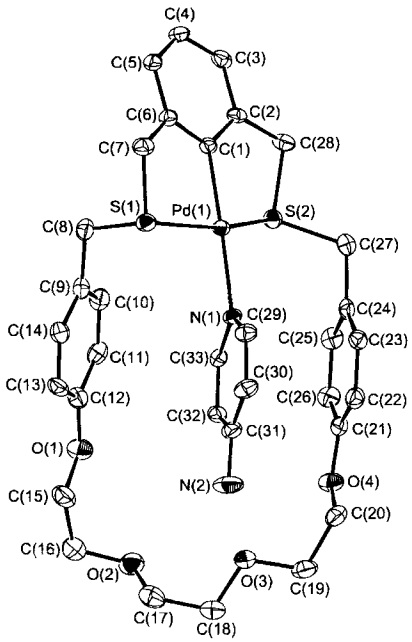

Figure 3. X-ray structure of complex **5** showing the atom numbering scheme. The model substrate *p*-aminopyridine is coordinated to the Pd atom, while stacking with *one* of the aromatic units and hydrogen bonding to the polyether unit; N(2)···O(3) 3.11(1) Å.

Table 5. Selected bond lengths (Å) and angles (°) for [Pd(**1**)(pap)][BF_4] (**5**).

Pd(1) S(1)	2.312(2)	Pd(1)–S(2)	2.300(2)
Pd(1)–N(1)	2.146(5)	Pd(1) C(1)	1.988(6)
S(1)–C(7)	1.818(6)	S(1)–C(8)	1.833(7)
S(2) C(27)	1.828(7)	S(2)–C(28)	1.836(6)
O(1) C(12)	1.370(8)	O(1)–C(15)	1.448(8)
O(2)- C(16)	1.406(9)	O(2)–C(17)	1.408(9)
O(3)–C(18)	1.421(8)	O(3)–C(19)	1.431(8)
O(4)–C(20)	1.433(8)	O(4)–C(21)	1.372(7)
N(1)–C(29)	1.339(8)	N(1)–C(33)	1.344(7)
N(2)–C(31)	1.376(8)	C(2)–C(28)	1.497(8)
C(6)–C(7)	1.497(9)	C(8)–C(9)	1.512(9)
C(15)–C(16)	1.50(1)	C(17) C(18)	1.48(1)
C(19)–C(20)	1.482(9)	C(24)–C(27)	1.507(9)
S(1)-Pd(1)-S(2)	160.00(6)	S(1)-Pd(1)-N(1)	91.2(1)
S(1)-Pd(1)-C(1)	84.8(2)	S(2)-Pd(1)-N(1)	101.1(1)
S(2)-Pd(1)-C(1)	83.5(2)	N(1)-Pd(1)-C(1)	175.3(2)
C(7)-S(1)-C(8)	98.4(3)	C(27)-S(2)-C(28)	101.2(3)
C(12)-O(1)-C(15)	116.8(6)	C(16)-O(2)-C(17)	115.1(6)
C(18)-O(3)-C(19)	112.5(5)	C(20)-O(4)-C(21)	118.3(5)
C(29)-N(1)-C(33)	116.5(5)	S(1)-C(7)-C(6)	109.7(5)
S(1)-C(8)-C(9)	112.5(5)	O(1)-C(15)-C(16)	107.0(7)
O(2)-C(16)-C(15)	113.4(7)	O(2)-C(17)-C(18)	109.7(6)
O(3)-C(18)-C(17)	109.7(6)	O(3)-C(19)-C(20)	110.0(6)
O(4)-C(20)-C(19)	108.3(6)	S(2)-C(27)-C(24)	110.2(4)
S(2)-C(28)-C(2)	108.1(4)		

© VCH Verlagsgesellschaft mbH, D-69451 Weinheim, 1997 0947-6539/97/0308-1206 $ 17.50+.50/0 Chem. Eur. J. 1997, 3, No. 8

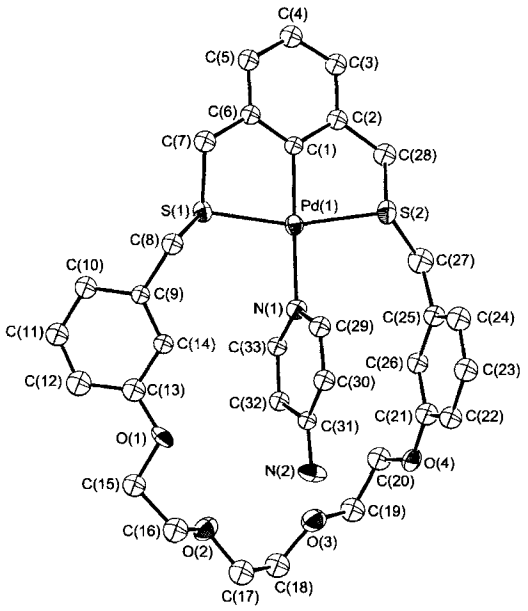

Figure 4. X-ray structure of complex **7**. The model substrate *p*-aminopyridine is coordinated to the Pd atom, while stacking with *one* of the aromatic units and hydrogen bonding to the polyether unit, N(2)···O(3) 3.13(5) Å.

Table 6. Selected bond lengths (Å) and angles (°) for [Pd(**2**)(pap)][BF_4] (**7**).

Pd(1)–S(1)	2.309(5)	Pd(1)–S(2)	2.305(5)
Pd(1)–N(1)	2.11(1)	Pd(1)–C(1)	2.00(2)
S(1)–C(7)	1.81(2)	S(1)–C(8)	1.83(2)
S(2)–C(27)	1.77(2)	S(2)–C(28)	1.84(2)
O(1)–C(13)	1.35(2)	O(1)–C(15)	1.44(2)
O(2)–C(16)	1.41(2)	O(2)–C(17)	1.41(2)
O(3)–C(18)	1.43(2)	O(3)–C(19)	1.40(2)
O(4)–C(20)	1.42(2)	O(4)–C(21)	1.33(2)
N(1)–C(29)	1.36(2)	N(1)–C(33)	1.31(2)
N(2)–C(31)	1.34(2)	C(2)–C(28)	1.50(2)
C(6)–C(7)	1.50(2)	C(8)–C(9)	1.51(2)
C(15)–C(16)	1.51(2)	C(17)–C(18)	1.44(2)
C(19)–C(20)	1.46(3)	C(25)–C(27)	1.56(2)
C(29)–C(30)	1.36(2)	C(30)–C(31)	1.38(2)
C(31)–C(32)	1.42(2)	C(32)–C(33)	1.37(2)
S(1)-Pd(1)-S(2)	163.8(2)	S(1)-Pd(1)-N(1)	98.2(4)
S(1)-Pd(1)-C(1)	82.5(5)	S(2)-Pd(1)-N(1)	97.7(4)
S(2)-Pd(1)-C(1)	81.5(5)	N(1)-Pd(1)-C(1)	178.3(6)
C(7)-S(1)-C(8)	101.6(8)	C(27)-S(2)-C(28)	100(1)
C(13)-O(1)-C(15)	118(2)	C(16)-O(2)-C(17)	114(2)
C(18)-O(3)-C(19)	116(2)	C(20)-O(4)-C(21)	119(2)
C(29)-N(1)-C(33)	117(2)	S(1)-C(7)-C(6)	108(1)
S(1)-C(8)-C(9)	112(1)	O(1)C(15)-C(16)	107(2)
O(2)-C(16)-C(15)	111(2)	O(2)-C(17)-C(18)	112(2)
O(3)-C(18)-C(17)	110(2)	O(3)-C(19)-C(20)	111(2)
O(4)-C(20)-C(19)	112(2)	S(2)-C(27)-C(25)	115(1)
S(2)-C(28)-C(2)	108(1)		

there is little perturbation of the Pd(S_2C) fragment and the bonding parameters associated with this unit are similar to those found for **5**. The receptor binding site *trans* to the Pd–C bond is occupied by the pap substrate, which is coordinated through the aromatic N atom. The *para*-amino group interacts with the polyether chain of the receptor, and an intramolecular hydrogen-bonding interaction occurs [H(N2A)···O(3) 2.40(1) Å, and N(2)–H(N2A)···O(3) 134(1)°]. An intermolecular hydrogen bond is also formed between substrate and anion [H(N2B)···F(3) 2.14(2) Å and N(2)–H(N2B)···F(1) 167.5(9)°]. This hydrogen-bonding scheme is also accompanied by the π stacking of *one* of the aromatic rings of the metalloreceptor with the aromatic ring of the pap substrate; the dihedral angle is 2.44°.

The only difference between the binding of pap in **5** and **7** is in the orientation of the *para*- or *meta*-substituted aromatic spacing unit *not* involved in π stacking to the substrate. For **5** the *para*-substituted aromatic spacer makes an angle of 37.3° with the pap substrate, while the same angle is 47.8° in **7**, where the spacing unit is *meta*-substituted. This difference is likely to be insignificant. These results with model substrates pap and map suggest that when the substrate is anchored to the metal at least one spacing unit can become involved in π stacking, while allowing for simultaneous hydrogen bonding. The different *para* and *meta* substitution patterns in the metalloreceptors do not appear to require significantly different binding modes, since both π stacking and hydrogen bonding are possible with either arrangement.

Synthesis and Characterization of Metalloreceptor–Purine Complexes: The addition of one equivalent of adenine or guanine to a solution of metalloreceptor in MeCN/MeOH resulted in isolation of the purine adducts [Pd(**1**)(adenine)][BF_4] (**13**), [Pd(**2**)(adenine)][BF_4] (**14**), [Pd(**1**)(guanine)][BF_4] (**15**) and [Pd(**2**)(guanine)][BF_4] (**16**). Although some features of the receptor–substrate interactions could be inferred from the ^{1}H NMR spectra, the poor solubility of these complexes, especially those of guanine, precluded a detailed analysis in solution. However, the solid state structures of **13**, **14** and **15b** were determined (Table 7) and yielded a great deal of insight into the interaction between these metalloreceptors and the nucleobases adenine and guanine.

Table 7. Summary of crystallographic data for complexes with DNA nucleobases.

	13	**14**	**15b** [c]
formula	$C_{33}H_{36}BF_4N_5O_4PdS_2$	$C_{33}H_{36}BF_3N_5O_4PdS_2$	$C_{34}H_{37}BCl_3F_3N_5O_5PdS_2$
M_r	824.00	824.00	1027.18
a, Å	11.725(3)	11.334(5)	14.589(6)
b, Å	13.755(3)	13.732(3)	20.444(6)
c, Å	10.809(3)	22.658(3)	14.849(4)
α, °	91.52(2)		
β, °	100.49(2)	101.61(2)	110.78(2)
γ, °	96.88(2)		
space group	$P\bar{1}$ (no. 2)	$P2_1/n$ (no. 14)	$P2_1/n$ (no. 14)
V, Å^3	1699.7(7)	3454(1)	4140(4)
ρ, gcm^{-3}	1.61	1.58	1.65
Z	2	4	4
μ, cm^{-1}	7.22	7.26	8.10
λ, Å	0.7017	0.7017	0.7017
T, °C	23	23	23
goodness of fit	1.69	2.06	2.51
$R(F_o)$, % [a]	4.49	5.29	5.11
$R_w(F_o)$, % [b]	5.77	6.26	5.92

[a] $R = \sum||F_o| - |F_c||/\sum|F_o||$. [b] $R_w = (\sum w(|F_o| - |F_c|)^2/\sum wF_o^2)^{1/2}$ and $w = 1/\sigma^2(F)$. [c] X-ray structure contains one molecule of $CHCl_3$ per molecule of complex.

From Scheme 6, it can be seen that adenine has three potential pairs of metal-coordination and hydrogen-bonding sites. Arrangement **A** involves N(3) and N(6) and is reminiscent of the observed interactions with *p*-aminopyridine, **B** utilizes N(1) and N(6), the sites employed in Watson–Crick base-pairing, and **C**

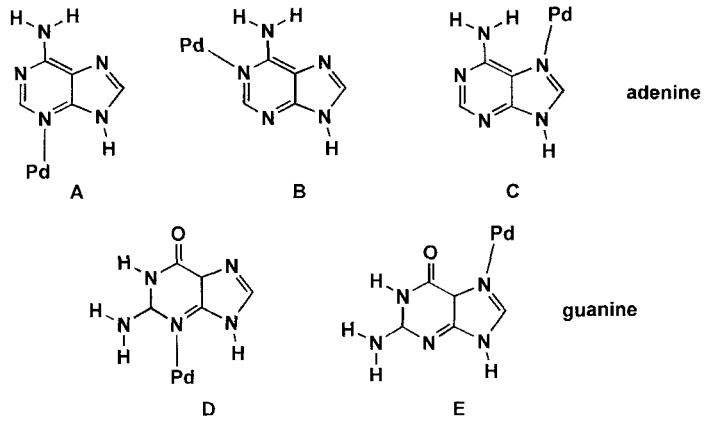

Scheme 6. DNA nucleobases adenine (**A**, **B**, **C**) and guanine (**D**, **E**) showing the possible metal-base interactions.

involves N(7) and N(6), the sites of Hoogsteen-type base-pairing. A perspective ORTEP drawing of **13**, in which adenine is bound to the Pd centre in receptor **3**, is shown in Figure 5 and some relevant bonding parameters are listed in Table 8.

The receptor binding site *trans* to the Pd–C bond is occupied by the adenine substrate, which is coordinated through N(3) of the six-membered aromatic ring. This orients the amino group towards the polyether chain of the receptor, and a pair of intramolecular hydrogen-bonding interactions occur [H(N6A)A···O(3) 2.251(8) Å, N(6)A–H(N6A)A···O(3) 159.1(6)° and H(N6A)A···O(2) 2.518(9) Å, N(6)A–H(N6A)A···O(2) 126.7(6)°]. This hydrogen-bonding scheme is accompanied by the π stacking of the planar adenine molecule between *both* the aromatic rings of the metalloreceptor, as is clearly illustrated in Figure 6.

Table 8. Selected bond lengths (Å) and angles (°) for [Pd(**1**)(adenine)][BF_4] (**13**).

Pd–S(1)	2.277(3)	Pd–S(2)	2.295(4)
Pd–N(3)A	2.129(7)	Pd–C(1)	1.99(1)
S(1)–C(7)	1.85(1)	S(1)–C(8)	1.82(1)
S(2)–C(27)	1.84(1)	S(2)–C(28)	1.80(1)
O(1)–C(12)	1.37(1)	O(1)–C(15)	1.42(1)
O(2)–C(16)	1.42(2)	O(2)–C(17)	1.33(2)
O(3)–C(18)	1.42(1)	O(3)–C(19)	1.41(1)
O(4)–C(20)	1.45(1)	O(4)–C(21)	1.39(1)
C(2)–C(28)	1.44(2)	C(6)–C(7)	1.42(2)
C(8)–C(9)	1.51(1)	C(15)–C(16)	1.48(2)
C(17)–C(18)	1.48(2)	C(19)–C(20)	1.49(2)
C(24)–C(27)	1.47(1)	C(4)A–C(5)A	1.41(1)
C(5)A–C(6)A	1.39(1)	N(1)A–C(2)A	1.34(1)
N(1)A–C(6)A	1.36(1)	N(3)A–C(2)A	1.34(1)
N(3)A–C(4)A	1.36(1)	N(6)A–C(6)A	1.36(1)
N(7)A–C(5)A	1.37(1)	N(7)A–C(8)A	1.34(1)
N(9)A–C(4)A	1.36(1)	N(9)A–C(8)A	1.33(1)
S(1)-Pd-S(2)	168.5(1)	S(1)-Pd-N(3)A	93.2(2)
S(1)-Pd-C(1)	85.2(4)	S(2)-Pd-N(3)A	98.1(2)
S(2)-Pd-C(1)	83.7(3)	N(3)A-Pd-C(1)	173.3(4)
Pd-S(1)-C(7)	99.8(4)	Pd-S(1)-C(8)	111.7(4)
C(7)-S(1)-C(8)	99.2(5)	Pd-S(2)-C(27)	113.5(4)
Pd-S(2)-C(28)	100.4(5)	C(27)-S(2)-C(28)	99.2(6)
C(12)-O(1)-C(15)	116.6(9)	C(16)-O(2)-C(17)	116(1)
C(18)-O(3)-C(19)	114(1)	C(20)-O(4)-C(21)	118.0(8)
S(1)-C(7)-C(6)	109.8(9)	S(1)-C(8)-C(9)	113.7(9)
O(1)-C(15)-C(16)	109(1)	O(2)-C(16)-C(15)	112(1)
O(2)-C(17)-C(18)	112(1)	O(3)-C(18)-C(17)	113(1)
O(3)-C(19)-C(20)	109(1)	O(4)-C(20)-C(19)	108(1)
S(2)-C(27)-C(24)	112.6(8)	S(2)-C(28)-C(2)	112(1)
C(2)A-N(1)A-C(6)A	117.3(8)	Pd-N(3)A-C(4)A	127.7(7)
Pd-N(3)A-C(2)A	118.9(6)	C(2)A-N(3)A-C(4)A	113.4(8)
C(5)A-N(7)A-C(8)A	103.5(9)	C(4)A-N(9)A-C(8)A	102.7(9)
N(1)A-C(2)A-N(3)A	128.6(9)	N(3)A-C(4)A-N(9)A	127.4(9)
N(3)A-C(4)A-C(5)A	123(1)	N(9)A-C(4)A-C(5)A	109.7(9)
N(7)A-C(5)A-C(4)A	107.0(9)	N(7)A-C(5)A-C(6)A	135(1)
C(4)A-C(5)A-C(6)A	118(1)	N(1)A-C(6)A-N(6)A	116.4(9)
N(1)A-C(6)A-C(5)A	119.6(9)	N(6)A-C(6)A-C(5)A	124(1)
N(7)A-C(8)A-N(9)A	117(1)		

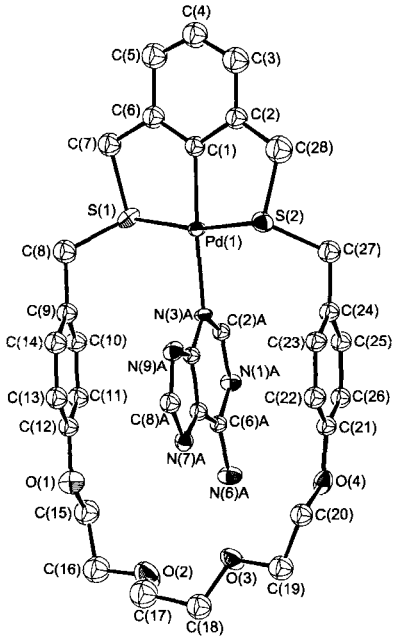

Figure 5. X-ray structure of complex **13** showing the atom numbering scheme. Adenine interacts with the metalloreceptor utilizing three different binding modes: 1) direct σ donation to the Pd centre through N(3)A, 2) π stacking of the planar, electron-poor base between the electron-rich aromatic units and 3) hydrogen bonding of the peripheral amino group [N(6)A, to crown ether oxygens at the base of the macrocycle. N(6)A···O(2) 3.18(1) Å, N(6)A···O(3) 3.16(1) Å].

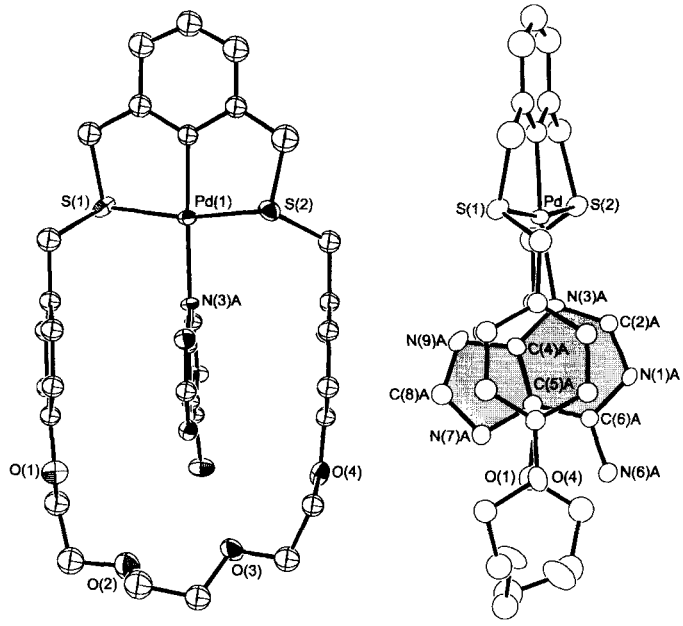

Figure 6. Two views of complex **13**. Left: parallel stacking (≈3.5 Å) of the adenine substrate between the *p*-aromatic spacing units of the metalloreceptor. Right: "offset" nature of the π stacking between the Pd-bound adenine substrate (shaded) and the *p*-aromatic spacing units of the metalloreceptor.

0947-6539/97/0308-1208 $ 17.50+.50/0 Chem. Eur. J. 1997, 3, No. 8

The binding mode observed for **13** corresponds to **A** in Scheme 6. As in the binding of pap, the coordination to N(3) orients the amino group for hydrogen bonding, while simultaneously allowing for π-stacking interactions. Interestingly, adenine–metal binding usually occurs through the more basic N(7) site.[111] In fact, this is only the second structurally characterized example of a monometallic adenine complex bonded through N(3). Houlton and co-workers recently reported the first example of a mononuclear complex of adenine bound through N(3) in which this atypical metal adenine interaction was *directed* by a chelating NCH_2CH_2N tether.[112] This supports the idea that hydrogen bonding in the second sphere can direct the nature of the metal–substrate interaction and is important in the metalloreceptor–substrate recognition event.

The significant difference between the binding of adenine and the binding of pap is that the electron-poor aromatic ring system of adenine can be oriented so that the fused-ring carbon atoms C(4) and C(5) are positioned exactly between the centres of the parallel aromatic rings of the receptor, an "offset" arrangement that optimizes the π–π interaction.[113] The three aromatic units are essentially parallel, with interplanar distances between receptor and substrate of approximately 3.35 Å and dihedral angles of 3.33 and 7.58°.

Exactly the same type of binding of adenine occurs when the aromatic spacing unit is *meta*-substituted. A perspective ORTEP drawing of **14** is shown in Figure 7, and some relevant bonding parameters are listed in Table 9.

The adenine substrate is coordinated through N(3), which orients the amino group towards the polyether chain of the receptor, and intramolecular hydrogen-bonding interactions

Table 9. Selected bond lengths (Å) and angles (°) for [Pd(**2**)(adenine)][BF_4] (**14**).

Pd–S(1)	2.286(3)	Pd–S(2)	2.296(3)
Pd–N(3)A	2.128(8)	Pd–C(1)	1.98(1)
S(1)–C(7)	1.82(1)	S(1)–C(8)	1.82(1)
S(2)–C(27)	1.83(1)	S(2)–C(28)	1.81(1)
O(1)–C(13)	1.34(1)	O(1)–C(15)	1.46(2)
O(2)–C(16)	1.39(2)	O(2)–C(17)	1.37(2)
O(3)–C(18)	1.18(2)	O(3)–C(19)	1.39(2)
O(4)–C(20)	1.43(2)	O(4)–C(21)	1.36(1)
C(2)–C(28)	1.48(2)	C(6)–C(7)	1.49(2)
C(8)–C(9)	1.51(2)	C(15)–C(16)	1.47(2)
C(17)–C(18)	1.45(2)	C(19)–C(20)	1.47(2)
C(25)–C(27)	1.50(1)	N(1)A–C(2)A	1.32(1)
N(1)A–C(6)A	1.33(1)	N(3)A–C(2)A	1.32(1)
N(3)A–C(4)A	1.35(1)	N(6)A–C(6)A	1.34(1)
N(7)A–C(5)A	1.36(1)	N(7)A–C(8)A	1.35(1)
N(9)A–C(4)A	1.36(1)	N(9)A–C(8)A	1.31(1)
C(5)A–C(4)A	1.37(1)	C(6)A–C(5)A	1.41(2)
S(1)-Pd(1)-S(2)	166.2(1)	S(1)-Pd(1)-N(3)A	95.6(2)
S(1)-Pd(1)-C(1)	84.0(3)	S(2)-Pd(1)-N(3)A	98.0(2)
S(2)-Pd(1)-C(1)	82.6(3)	N(3)A-Pd(1)-C(1)	176.7(4)
Pd(1)-S(1)-C(7)	100.1(4)	Pd(1)-S(1)-C(8)	108.4(4)
C(7)-S(1)-C(8)	99.6(6)	Pd(1)-S(2)-C(27)	114.0(4)
Pd(1)-S(2)-C(28)	97.8(4)	C(27)-S(2)-C(28)	101.0(6)
C(13)-O(1)-C(15)	116(1)	C(16)-O(2)-C(17)	114(1)
C(18)-O(3)-C(19)	124(2)	C(20)-O(4)-C(21)	117(1)
S(1)-C(7)-C(6)	108.7(9)	S(1)-C(8)-C(9)	110.7(9)
O(1)-C(15)-C(16)	107(1)	O(2)-C(16)-C(15)	111(1)
O(2)-C(17)-C(18)	112(1)	O(3)-C(18)-C(17)	127(2)
O(3)-C(19)-C(20)	109(2)	O(4)-C(20)-C(19)	109(1)
S(2)-C(27)-C(25)	111.6(9)	S(2)-C(28)-C(2)	108.2(9)
C(2)A-N(1)A-C(6)A	118(1)	Pd(1)-N(3)A-C(4)A	124.8(8)
Pd(1)-N(3)A-C(2)A	122.9(8)	C(2)A-N(3)A-C(4)A	112(1)
C(5)A-N(7)A-C(8)A	103.1(9)	C(4)A-N(9)A-C(8)A	104(1)
N(3)A-C(2)A-N(1)A	129(1)	N(3)A-C(4)A-N(9)A	127(1)
N(3)A-C(4)A-C(5)A	125(1)	N(9)A-C(4)A-C(5)A	109(1)
N(7)A-C(5)A-C(6)A	135(1)	N(7)A-C(5)A-C(4)A	109(1)
C(6)A-C(5)A-C(4)A	117(1)	N(1)A-C(6)A-N(6)A	118(1)
N(1)A-C(6)A-C(5)A	119(1)	N(6)A-C(6)A-C(5)A	123(1)
N(7)A-C(8)A-N(9)A	115(1)		

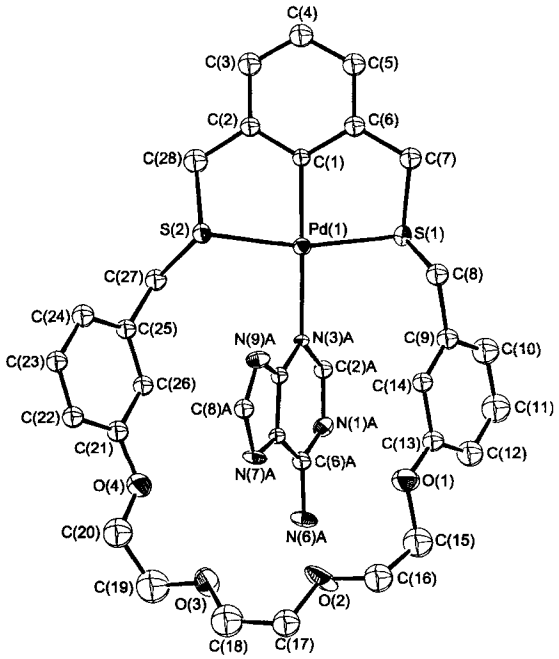

Figure 7. X-ray structure of complex **14** showing the atom numbering scheme. Adenine interacts with the metalloreceptor utilizing three different binding modes: 1) direct σ donation to the Pd centre through N(3)A, 2) π stacking of the planar, electron-poor base between the electron-rich aromatic units and 3) hydrogen bonding of the peripheral amino group, N(6)A, to crown ether oxygens at the base of the macrocycle [N(6)A···O(2) 3.00(1) Å, N(6)A···O(3) 3.26(1) Å].

occur [H(N6B)A···O(2) 2.257(9) Å, N(6)A–H(N6B)A···O(2) 134.3(7)° and H(N6B)A···O(3) 2.41(1) Å, N(6)A–H(N6B)A···O(3) 149.7(7)°]. This hydrogen-bonding scheme is also accompanied by the π stacking of *both* of the aromatic rings of the metalloreceptor with the fused aromatic ring system of the adenine substrate (dihedral angles of 9.08 and 13.44°). This receptor containing the *meta* aromatic spacing units does not appear to allow all three interaction types to optimize as well as the *para* compound. This is clearly illustrated by the two views shown in Figure 8.

Scheme 6 shows that guanine has only two potential pairs of metal-coordination and hydrogen-bonding sites. Mode **D** involves N(3) and N(2), while **E** makes use of N(7) and N(2). In our attempts to grow X-ray quality crystals of **15**, crystals of a complex **15b**, containing an N(9)-substituted BF_3 adduct of guanine, were isolated. Although the source of the BF_3 group must certainly be the BF_4^- anion of the metalloreceptor, attempts to rationally synthesize this side product and determine the mechanism of formation have been unsuccessful to date. A perspective ORTEP drawing of **15b**, in which the guanine derivative is bound to the Pd centre in receptor **3**, is shown in Figure 9, and some relevant bonding parameters are listed in Table 10.

The receptor binding site *trans* to the Pd–C bond is occupied by the N(7) atom of the five-membered aromatic ring. This orients the amino group on the opposite side of the six-mem-

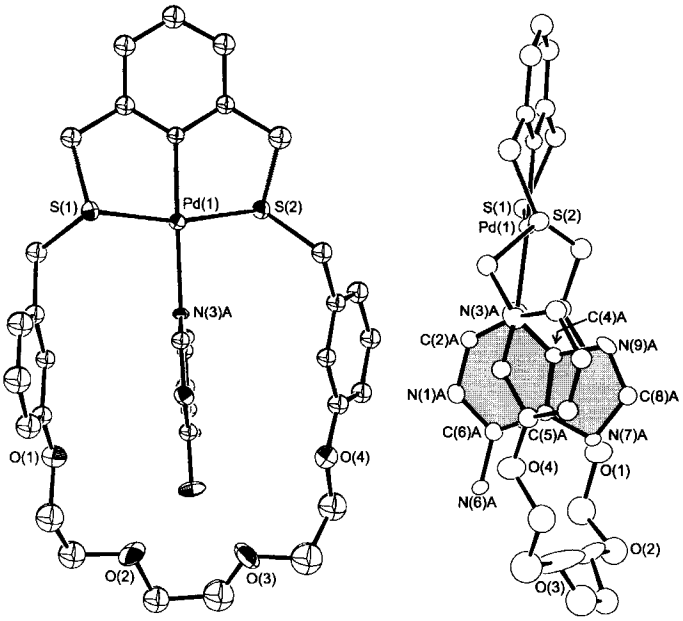

Figure 8. Two views of complex **14**. Left: parallel stacking (≈ 3.5 Å) of the adenine substrate between the *m*-aromatic spacing units of the metalloreceptor. Right: "off-set" nature of the π stacking between the Pd-bound adenine substrate (shaded) and the *m*-aromatic spacing units of the metalloreceptor.

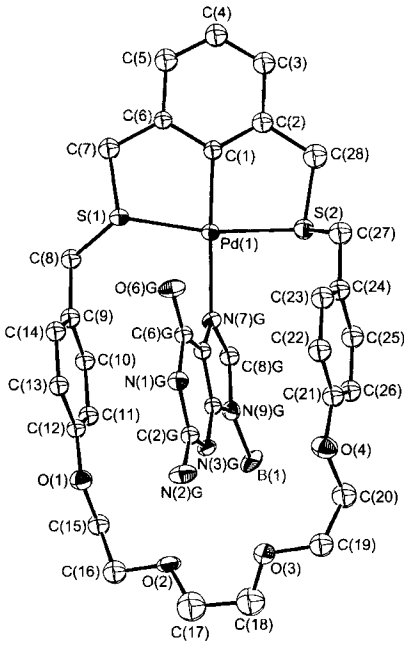

Figure 9. X-ray structure of complex **15b** showing the atom numbering scheme. The guanine derivative interacts with the metalloreceptor as follows: 1) direct σ donation to the Pd centre through N(7)G, 2) π stacking of the planar, electron-poor base between the electron-rich aromatic units and 3) hydrogen bonding of the peripheral amino group, N(2)G, to crown ether oxygens at the base of the macrocycle [N(2)G $\cdots$ O(2) 3.16(1) Å, N(2)G $\cdots$ O(3) 2.87(1) Å].

bered ring towards the polyether chain of the receptor, and a pair of intramolecular bifurcated hydrogen bonds occur [H(N2B)G $\cdots$ O(2) 2.479(9) Å, N(2)G–H(N2B)G $\cdots$ O(2) 128.5(6)° and H(N2B)G $\cdots$ O(3) 2.140(8) Å, N(2)G–H(N2B)G $\cdots$ O(3) 132.9(6)°]. This hydrogen-bonding scheme is accompanied by the π stacking of *both* of the aromatic rings of the metalloreceptor with the fused aromatic ring system of

Table 10. Selected bond lengths (Å) and angles (°) for [Pd(**1**)(guanine-BF_3)][BF_4]. $CHCl_3$ (**15b**).

Pd–S(1)	2.297(3)	Pd–S(2)	2.294(3)
Pd–N(7)G	2.153(7)	Pd–C(1)	2.00(1)
S(1)–C(7)	1.84(1)	S(1)–C(8)	1.83(1)
S(2)–C(27)	1.82(1)	S(2)–C(28)	1.81(1)
O(1)–C(12)	1.36(1)	O(1)–C(15)	1.44(1)
O(2)–C(16)	1.41(1)	O(2)–C(17)	1.31(2)
O(3)–C(18)	1.34(2)	O(3)–C(19)	1.41(1)
O(4)–C(20)	1.40(1)	O(4)–C(21)	1.39(1)
O(6)G–C(6)G	1.23(1)	N(7)G–C(5)G	1.39(1)
N(7)G–C(8)G	1.31(1)	N(1)G–C(6)G	1.42(1)
N(1)G–C(2)G	1.36(1)	N(3)G–C(2)G	1.32(1)
N(3)G–C(4)G	1.38(1)	N(9)G–C(4)G	1.34(1)
N(9)G–C(8)G	1.37(1)	N(2)G–C(2)G	1.32(1)
C(2)–C(28)	1.53(1)	C(6)–C(7)	1.47(1)
C(8)–C(9)	1.50(1)	C(15)–C(16)	1.49(1)
C(17)–C(18)	1.47(2)	C(19)–C(20)	1.51(2)
C(5)G–C(4)G	1.38(1)	C(24)–C(27)	1.50(1)
C(5)G–C(6)G	1.38(1)		
S(1)-Pd-S(2)	168.6(1)	S(1)-Pd-N(7)G	98.4(2)
S(1)-Pd-C(1)	84.5(3)	S(2)-Pd-N(7)G	92.3(2)
S(2)-Pd-C(1)	84.9(3)	N(7)G-Pd-C(1)	177.1(4)
C(7)-S(1)-C(8)	100.9(5)	C(27)-S(2)-C(28)	98.9(5)
C(12)-O(1)-C(15)	117.5(8)	C(16)-O(2)-C(17)	116(1)
C(18)-O(3)-C(19)	116(1)	C(20)-O(4)-C(21)	118(1)
C(5)G-N(7)G-C(8)G	106.1(8)	C(2)G-N(1)G-C(6)G	126.1(9)
C(2)G-N(3)G-C(4)G	120.1(8)	C(4)G-N(9)G-C(8)G	103.5(8)
S(1)-C(7)-C(6)	106.1(7)	S(1)-C(8)-C(9)	111.6(8)
O(1)-C(15)-C(16)	108.4(9)	O(2)-C(16)-C(15)	110(1)
O(2)-C(17)-C(18)	116(1)	O(3)-C(18)-C(17)	113(1)
O(3)-C(19)-C(20)	112(1)	O(4)-C(20)-C(19)	108(1)
S(2)-C(27)-C(24)	113.3(8)	S(2)-C(28)-C(2)	109.9(8)
N(7)G-C(5)G-C(6)G	131.6(9)	N(7)G-C(5)G-C(4)G	105.6(8)
C(6)G-C(5)G-C(4)G	123(1)	O(6)G-C(6)G-N(1)G	117(1)
N(1)G-C(2)G-N(3)G	118(1)	N(1)G-C(6)G-C(5)G	112.0(9)
N(3)G-C(2)G-N(2)G	122(1)	N(1)G-C(2)G-N(2)G	122(1)
N(3)G-C(4)G-C(5)G	120.6(9)	N(3)G-C(4)G-N(9)G	128.3(9)
N(7)G-C(8)G-N(9)G	113.5(9)	N(9)G-C(4)G-C(5)G	111.0(9)

guanine (dihedral angles are 1.90 and 2.97°). The orientation of the aromatic rings in this stacking interaction is clearly illustrated in Figure 10, and the binding mode corresponds to **E** in

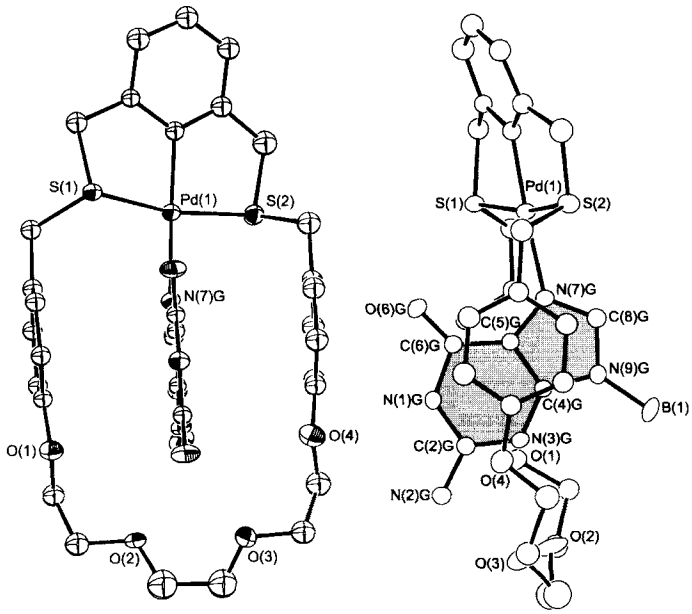

Figure 10. Two views of complex **15b**. Left: parallel stacking (≈ 3.5 Å) of the guanine derivative between the *p*-aromatic spacing units of the metalloreceptor. Right: "off-set" nature of the π stacking between the Pd-bound guanine derivative (shaded) and the *p*-aromatic spacing units of the metalloreceptor.

0947-6539/97/0308-1210 $ 17.50+.50/0 Chem. Eur. J. 1997, 3, No. 8

Scheme 6. The overall "fit" of guanine into this metalloreceptor is quite impressive, with all three types of interactions exhibiting nearly ideal interaction parameters.

Conclusion

The metalloreceptors studied in this work were designed to employ the complimentary interactions of metal coordination, hydrogen bonding and π stacking. It is evident from NMR spectroscopic studies that all three of these interactions can occur in solution. The solid state structures presented allow an examination of the separate components and an evaluation of how the interactions operate in concert in a molecular recognition event.

Experimental Section

All starting materials—triethylene glycol di-*p*-tosylate, 4-hydroxybenzyl alcohol, 3-hydroxybenzyl alcohol, *m*-xylene-α,α'-dithiol, *p*-aminopyridine (pap), *m*-aminopyridine (map), pyridine (py), guanine, adenine, deuterated solvents and anhydrous *N,N'*-dimethylformamide (DMF)—were purchased from Aldrich Chemicals. All reactions were performed under an atmosphere of N_2(g) using standard Schlenk or dry-box techniques, and all solvents and liquid starting materials were dried and degassed prior to use. ^{1}H and ^{13}C NMR spectra were recorded on a Brüker AC 300 spectrometer locked to the deuterated solvent at 300.1 and 75.5 MHz respectively, and infrared spectra were recorded on a Nicolet 5DX or BOMEM Michelson 100 FTIR spectrometer. LSIMS data were obtained on a Kratos Profile mass spectrometer. Elemental analyses were performed by Canadian Microanalytical Service, Delta, British Columbia.

Triethylene glycol di-*p*-hydroxybenzyl ether: 4-Hydroxybenzyl alcohol (10.8 g, 87.0 mmol) was added to a solution of Na (2.00 g, 87.0 mmol) dissolved in anhydrous ethanol (200 mL). Triethylene glycol di-*p*-tosylate (19.9 g, 43.5 mmol) was added slowly, and the solution refluxed for 22 h. The resulting mixture was filtered to remove sodium tosylate, and the solvent removed in vacuo. The resulting solid residue was extracted with CH_2Cl_2 (100 mL), and this organic fraction extracted with H_2O (2 × 50 mL) and then dried over anhydrous $MgSO_4$. After filtration and removal of solvent, the crude product was isolated and recrystallized from CH_2Cl_2. Yield 11.5 g (73%). ^{1}H NMR ($CDCl_3$): δ = 7.23 (d, 4H, J = 8.3 Hz, Ar), 6.87 (d, 4H, J = 8.3 Hz, Ar), 4.57 (s, 4H, Bz), 4.10 (t, 4H, J = 4.7 Hz, $ArOCH_2$), 3.84 (t, 4H, J = 4.7 Hz, OCH_2), 3.73 (s, 4H, OCH_2), 1.77 (br s, 2H, OH). ^{13}C{^{1}H} NMR ($CDCl_3$): δ = 158.53, 133.43, 128.68, 114.83 (Ar), 70.99, 69.90, 67.61 (OCH_2), 65.10 (Bz). Anal. calcd for $C_{20}H_{26}O_6$: C 66.27; H 7.24. Found: C 66.20; H 7.19.

Triethylene glycol di-*m*-hydroxybenzyl ether: The same procedure was employed as described for triethylene glycol di-*p*-hydroxybenzyl ether, except that 3-hydroxybenzyl alcohol was substituted for 4-hydroxybenzyl alcohol. Yield 16.13 g (93%). ^{1}H NMR ($CDCl_3$): δ = 7.21–6.79 (m, 8H, Ar), 4.59 (s, 4H, Bz), 4.09 (t, 4H, J = 4.8 Hz, OCH_2), 3.83 (t, 4H, J = 4.8 Hz, OCH_2), 3.72 (s, 4H, OCH_2); ^{13}C{^{1}H} NMR ($CDCl_3$): δ = 155.95, 135.97, 129.96, 119.30, 114.71, 113.89 (Ar), 71.00, 69.91, 67.59 (OCH_2), 64.99 (Bz). Anal. calcd for $C_{20}H_{26}O_6$: C 66.27; H 7.24. Found: C 66.22; H 7.19.

Triethylene glycol di-*p*-chlorobenzyl ether: A solution of $SOCl_2$ (1.97 g, 16.6 mmol) in CH_2Cl_2 (50 mL) was added a solution of triethylene glycol di-*p*-hydroxybenzyl ether (3.00 g, 8.28 mmol) and pyridine (1.31 g, 16.6 mmol) in CH_2Cl_2 (50 mL). The addition was performed over a period of 3 h, and the solution was allowed to stir for a further 22 h. The volume of the CH_2Cl_2 solution was reduced to 50 mL and then extracted with H_2O (2 × 50 mL) and 0.1 M NaOH (2 × 50 mL). The organic fraction was then dried over anhydrous $MgSO_4$. After filtration and removal of the solvent, the crude solid was recrystallized from CH_2Cl_2. Yield 2.02 g (61%). ^{1}H NMR ($CDCl_3$): δ = 7.27 (d, 4H, J = 8.6 Hz, Ar), 6.86 (d, 4H, J = 8.6 Hz, Ar), 4.53 (s, 4H, Bz), 4.10 (t, 4H, J = 4.8 Hz, OCH_2), 3.84 (t, 4H, J = 4.8 Hz, OCH_2), 3.73 (s, 4H, OCH_2). ^{13}C{^{1}H} NMR ($CDCl_3$): δ = 158.84, 129.99, 129.65, 114.79 (Ar), 70.85 (OCH_2), 69.69 (OCH_2), 67.46 (OCH_2), 46.23 (Bz). Anal. calcd for $C_{20}H_{24}Cl_2O_4$: C 60.14; H 6.07. Found: C 60.09; H 6.00.

Triethylene glycol di-*m*-chlorobenzyl ether: The same procedure was employed as described for triethylene glycol di-*p*-chlorobenzyl ether, except that triethylene glycol di-*m*-hydroxybenzyl ether was substituted for triethylene glycol di-*p*-hydroxybenzyl ether. Yield 9.23 g (84%). ^{1}H NMR ($CDCl_3$): δ = 7.22-6.85 (m, 8H, Ar), 4.51 (s, 4H, Bz), 4.11 (t, 4H, J = 4.8 Hz, OCH_2), 3.84 (t, 4H, J = 4.8 Hz, OCH_2), 3.73 (s, 4H, OCH_2). ^{13}C{^{1}H} NMR ($CDCl_3$): δ = 159.12, 138.97, 129.85, 121.10, 114.93, 114.81 (Ar), 71.00, 69.87, 67.58 (OCH_2), 46.29 (Bz). Anal. calcd for $C_{20}H_{24}Cl_2O_4$: C 60.14; H 6.07. Found: C 60.11; H 6.02.

Thiacyclophane (1): Cesium carbonate (7.65 g, 23.4 mmol) was suspended in DMF (400 mL) under an atmosphere of N_2(g). To this mixture was added triethylene glycol di-*p*-chlorobenzyl ether (4.69 g, 11.7 mmol) and *m*-xylene-α,α'-dithiol (2.00 g, 11.7 mmol) in DMF (200 mL). The addition was performed over a period of 48 h with the reaction temperature maintained at 55–60 °C. After addition, the DMF was removed under vacuum and the resulting solid residue extracted with CH_2Cl_2 (150 mL). This CH_2Cl_2 solution was extracted with H_2O (1 × 50 mL) and 0.1 M NaOH (2 × 50 mL), and then the organic fractions were dried over anhydrous $MgSO_4$. After filtration and removal of the solvent, the crude product was recrystallized from CH_2Cl_2/ethanol. Yield 2.69 g (46%). ^{1}H NMR ($CDCl_3$): δ = 7.30 (s, 3H, Ar), 7.12 (d, 4H, J = 8.4 Hz, *p*-Ar), 6.83 (s, 1H, Ar), 6.80 (d, 4H, J = 8.4 Hz, *p*-Ar), 4.08 (t, 4H, J = 4.6 Hz, OCH_2), 3.88 (t, 4H, J = 4.6 Hz, OCH_2), 3.74 (s, 4H, OCH_2), 3.51 (s, 4H, Bz), 3.49 (s, 4H, Bz). ^{13}C{^{1}H} NMR ($CDCl_3$): δ = 157.87, 137.83, 130.27, 130.02, 129.08, 127.50, 114.73 (Ar), 70.97, 69.72, 67.59 (OCH_2), 34.82, 34.49 (Bz). Anal. calcd for $C_{28}H_{32}O_4S_2$: C 67.70; H 6.51. Found: C 67.57; H 6.44.

Thiacyclophane (2): The same procedure as described for **1** was employed, except triethylene glycol di-*m*-chlorobenzyl ether was substituted for triethylene glycol di-*p*-chlorobenzyl ether. Yield 2.53 g (44%). ^{1}H NMR ($CDCl_3$): δ = 7.24–6.76 (m, 12H, Ar), 4.05 (t, 4H, J = 4.6 Hz, OCH_2), 3.82 (t, 4H, J = 4.6 Hz, OCH_2), 3.72 (s, 4H, OCH_2), 3.58 (s, 8H, Bz). ^{13}C{^{1}H} NMR ($CDCl_3$): δ = 158.85, 139.53, 38.11, 129.60, 129.44, 128.76, 127.60, 121.42, 115.17, 113.46 (Ar), 70.98, 69.82, 67.46 (OCH_2), 35.86, 35.67 (Bz). Anal. calcd for $C_{28}H_{32}O_4S_2$: C 67.70; H 6.51. Found: C 67.60; H 6.41.

[Pd(1)(MeCN)][BF$_4$] (3): Thiacyclophane **1** (0.28 g, 5.6 mmol) was dissolved in acetonitrile (60 mL) and heated to reflux. To this solution was added $[Pd(MeCN)_4][BF_4]_2$ (250 mg, 5.6 mmol) in acetonitrile (10 mL). The resulting solution was stirred and refluxed for a further 22 h. The acetonitrile was removed and the resulting solid residue recrystallized from CH_2Cl_2/acetonitrile. Yield 250 mg (76%). ^{1}H NMR ($CDCl_3$): δ = 7.35 (d, 4H, J = 8.6 Hz, *p*-Ar), 6.92 (m, 3H, Pd–Ar), 6.87 (d, 4H, J = 8.6 Hz, *p*-Ar), 4.31 (br s, 8H, Bz), 4.11 (t, 4H, J = 4.1 Hz, OCH_2), 3.77 (t, 4H, J = 4.1 Hz, OCH_2), 3.61 (s, 4H, OCH_2). Anal. calcd for $C_{30}H_{34}BF_4NO_4PdS_2$: C 49.36; H 4.70. Found: C 49.14; H 4.52.

[Pd(2)(MeCN)][BF$_4$] (4): The same procedure as described for **3** was employed except **2** was used in place of **1**. Yield 290 mg (88%). ^{1}H NMR ($CDCl_3$): δ = 7.26–6.85 (m, 11H, Ar), 4.30 (s, 8H, Bz), 4.18 (t, 4H, J = 4.0 Hz, OCH_2), 3.82 (t, 4H, J = 4.0 Hz, OCH_2), 3.66 (s, 4H, OCH_2). Anal. calcd for $C_{30}H_{34}BF_4NO_4PdS_2$: C 49.36; H 4.70. Found: C 49.19; H 4.61.

[Pd(1)(pap)][BF$_4$] (5): Complex **3** (25.0 mg, 0.034 mmol) and *p*-aminopyridine (pap) (3.2 mg, 0.034 mmol) were added to acetonitrile (5 mL) and stirred for 24 h. The solvent was evaporated and the resulting solid residue recrystallized from $CHCl_3$/acetonitrile. Yield 24.9 mg (93%). ^{1}H NMR ($CDCl_3$): δ = 7.03 (m, 3H, Pd–Ar), 6.99 (d, 4H, J = 8.5 Hz, *p*-Ar), 6.74 (d, 2H, J = 6.4 Hz, pap-Ar), 6.45 (d, 4H, J = 8.5 Hz, *p*-Ar), 5.91 (d, 2H, J = 6.4 Hz, pap-Ar), 5.39 (s, 2H, NH_2), 4.49 (s, 4H, Bz), 4.24 (s, 4H, Bz), 3.99 (t, 4H, $ArOCH_2$), 3.77 (t, 4H, OCH_2), 3.71 (s, 4H, OCH_2). Anal. calcd for $C_{33}H_{37}BF_4N_2O_4PdS_2$: C 50.62; H 4.77. Found: C 50.55; H 4.70.

[Pd(1)(map)][BF$_4$] (6): The same procedure as described for **5** was employed except that *m*-aminopyridine (map) was substituted for *p*-aminopyridine. Yield 25.1 mg (94%). ^{1}H NMR ($CDCl_3$): δ = 7.44 (s, 1H, map-Ar), 7.41 (d, 4H, J = 8.6 Hz, *p*-Ar), 7.41 (s, 1H, map-Ar), 7.01 (m, 2H, map-Ar), 6.94 (m,

3H, Pd–Ar), 6.89 (d, 4H, *p*-Ar), 4.51 (brs, 2H, NH_2), 4.35 (s, 8H, Bz), 4.10 (s, 4H, OCH_2), 3.74 (m, 4H, OCH_2), 3.56 (s, 4H, OCH_2). Anal. calcd for $C_{33}H_{37}BF_4N_2O_4PdS_2$: C 50.62; H 4.77. Found: C 50.47; H 4.68.

[Pd(2)(pap)][BF_4] (7): The same procedure as described for **5** was employed except that **4** was substituted for **3**. Yield 26.5 mg (100%). ^{1}H NMR ($CDCl_3$): δ = 7.16 (m, 2H, *m*-Ar), 7.10 (d, 2H, J = 6.3 Hz, pap), 7.05 (m, 3H, Pd–Ar), 6.84 (d, 2H, *m*-Ar), 6.69 (d, 2H, *m*-Ar), 6.62 (s, 2H, *m*-Ar), 6.27 (d, 2H, J = 6.3 Hz, pap), 5.28 (s, 2H, NH_2), 4.49 (s, 4H, Bz), 4.21 (s, 4H, Bz), 4.05 (t, 4H, OCH_2), 3.79 (t, 4H, OCH_2), 3.72 (s, 4H, OCH_2). Anal. calcd for $C_{33}H_{37}BF_4N_2O_4PdS_2$: C 50.62; H 4.77. Found: C 50.50; H 4.66.

[Pd(2)(map)][BF_4] (8): The same procedure as described for **6** was employed except that **4** was substituted for **3**. Yield 24.8 mg (93%). ^{1}H NMR ($CDCl_3$): δ = 7.08 (m, 2H, map), 6.99 (m, 3H, Pd Ar), 6.96-6.55 (m, 10H, *m*-Ar, map), 4.45 (s, 2H, NH_2), 4.25 (s, 8H, Bz), 4.05 (s, 4H, OCH_2), 3.72 (s, 4H, OCH_2), 3.52 (s, 4H, OCH_2). Anal. calcd for $C_{33}H_{37}BF_4N_2O_4PdS_2$: C 50.62; H 4.77. Found: C 50.58; H 4.75.

1,3-Bis(*n*-butylthiomethyl)benzene (9): *n*-Butanethiol (3.15 g, 38 mmol) was added to anhydrous ethanol (100 mL), in which Na metal (0.87 g, 38 mmol) had been dissolved. This mixture was stirred for 4 h. α,α'-Dibromo-*m*-xylene (5.00 g, 19 mmol) was added and the reaction mixture stirred for a further 4 h. The ethanol was removed and the resulting pale yellow oil extracted with CH_2Cl_2 (50 mL). The organic solution was washed with water (2 × 50 mL) and then dried over anhydrous $MgSO_4$. Removal of the CH_2Cl_2 gave a clear colourless oil. Yield 5.08 g, (95%). ^{1}H NMR ($CDCl_3$): δ = 7.24 7.14 (m, 4H, Ar), 3.66 (s, 4H, Bz), 2.38 (t, 4H, SCH_2), 1.52 (qnt, 4H, CH_2), 1.33 (sxt, 4H, CH_2), 0.86 (t, 6H, CH_3). Anal. calcd for $C_{16}H_{26}S_2$: C 68.01; H 9.29. Found: C 67.92; H 9.22.

[Pd(9)(MeCN)][BF_4] (10): $[Pd(MeCN)_4][BF_4]_2$ (513 mg, 1.15 mmol) and **9** (326 mg, 1.15 mmol) were combined in MeCN (50 mL) and the mixture stirred for 8 h. The solution turned form orange to bright yellow in colour. Diethyl ether (40 mL) was added and the resulting yellow precipitate isolated by filtration. Yield 344 mg (58%). ^{1}H NMR ($CDCl_3$): δ = 7.09 (m, 3H, Pd–Ar), 4.13 (br, s, 4H, Bz), 3.25 (t, 4H, SCH_2), 2.26 (s, 3H, MeCN), 1.77 (qnt, 4H, CH_2), 1.46 (sxt, 4H, CH_2), 0.90 (t, 6H, CH_3). Anal. calcd for $C_{18}H_{28}BF_4NPdS_2$: C 41.91; H 5.48. Found: C 41.77; H 5.39.

[Pd(9)(pap)][BF_4] (11): **10** (21.2 mg, 0.041 mmol) and *p*-aminopyridine (pap) (3.9 mg, 0.041 mmol) were added to acetonitrile (10 mL) and stirred for 24 h. The solvent was evaporated and the resulting solid residue recrystallized from MeCN. Yield 23.1 mg (99%). ^{1}H NMR (CD_3CN): δ = 8.04 (d, 2H, J = 5.6 Hz, pap-Ar), 6.99 (m, 3H, Pd–Ar), 6.64 (d, 2H, J = 5.6 Hz, pap-Ar), 5.14 (s, 2H, NH_2), 4.33 (s, 4H, Bz), 2.89 (s, 4H, SCH_2), 1.61 (s, 4H, CH_2), 1.30 (m, 4H, CH_2), 0.86 (m, 6H, CH_3). Anal. calcd for $C_{20}H_{31}BF_4N_2PdS_2$: C 43.13; H 5.62. Found: C 42.99; H 5.57.

[Pd(9)(map)][BF_4] (12): Compound **10** (31.3 mg, 0.061 mmol) and *m*-aminopyridine (map) (5.7 mg, 0.061 mmol) were added to acetonitrile (10 mL) and stirred for 24 h. The solvent was evaporated and the resulting solid residue recrystallized from MeCN. Yield 33.7 mg (97%). ^{1}H NMR (CD_3CN): δ = 8.04 (s, 1H, map-Ar), 7.88 (d, 1H, map-Ar), 7.16 (m, 2H, map-Ar), 7.00 (m, 3H, Pd–Ar), 4.72 (s, 2H, NH_2), 4.32 (s, 4H, Bz), 2.90 (s, 4H, SCH_2), 1.60 (s, 4H, CH_2), 1.29 (m, 4H, CH_2), 0.79 (m, 6H, CH_3). Anal. calcd for $C_{20}H_{21}BF_4N_2PdS_2$: C 43.13; H 5.62. Found: C 43.00; H 5.51.

[Pd(1)(adenine)][BF_4] (13): Compound **3** (25.0 mg, 0.034 mmol) and adenine (4.6 mg, 0.034 mmol) were stirred in MeCN (5 mL) and CH_3OH (5 mL) for 24 h. The solvents were removed in *vacuo* to yield a light yellow solid. The solid was washed with diethyl ether (5 mL) and recrystallized from MeCN/diethyl ether. Yield 22.1 mg (79%). ^{1}H NMR (CD_3CN): δ = 10.40 (s, 1H, NH), 7.95 (s, 1H, H(8A)), 7.73 (s, 1H, H(2A)), 7.04 (m, 3H, Pd–Ar), 6.74 (d, 4H, J = 7.9 Hz, *p*-Ar), 6.19 (brs, 2H, NH_2), 6.01 (d, 4H, J = 7.9 Hz, *p*-Ar), 4.55 (brs, 4H, Bz), 4.24 (s, 4H, Bz), 3.85 (m, 12H, OCH_2). Anal. calcd for $C_{33}H_{36}BF_4N_5O_4PdS_2$: C 40.81; H 3.80. Found: C 40.64; H 3.68.

[Pd(2)(adenine)][BF_4] (14): Compound **4** (25.0 mg, 0.034 mmol) and adenine (4.6 mg, 0.034 mmol) were stirred in MeCN (5 mL) and CH_3OH (5 mL) for 24 h. The solution was filtered to remove a small amount of unreacted adenine and the product precipitated by the addition of diethyl ether (10 mL). The solid was washed with diethyl ether (5 mL) and recrystallized by slow evaporation of a MeCN solution of the compound. Yield 22.4 mg (80%). ^{1}H NMR (CD_3CN): δ = 10.39 (s, 1H, NH), 7.95 (s, 1H, H(8A)), 7.73 (s, 1H, H(2A)), 7.02 (m, 3H, Pd–Ar), 6.74 (d, 4H, J = 8.0 Hz, *p*-Ar), 6.19 (brs, 2H, NH_2), 6.01 (d, 4H, J = 8.0 Hz, *p*-Ar), 4.55 (brs, 4H, Bz), 4.24 (s, 4H, Bz), 3.85 (m, 12H, OCH_2). Anal. calcd for $C_{33}H_{36}BF_4N_5O_4PdS_2$: C 40.81; H 3.80. Found: C 40.57; H 3.70.

[Pd(1)(guanine)][BF_4] (15a): Compound **3** (25.0 mg, 0.034 mmol) was dissolved in MeCN (5 mL), and guanine (5.2 mg, 0.034 mmol) in CH_3OH (5 mL) was added with stirring. After 24 h, an off-white solid was isolated by filtration. Yield 18.6 mg (65%). ^{1}H NMR ($CDCl_3$): δ = 9.81 (s, 1H, NH), 8.59 (s, 1H, NH), 7.23 (d, 4H, J = 8.3 Hz, *p*-Ar; overlap with 1H, H(8)G), 7.01 (m, 3H, Pd–Ar), 6.38 (d, 4H, J = 8.3 Hz, *p*-Ar), 5.67 (s, 2H, NH_2), 4.31 (s, 8H, Bz), 4.12 (s, 4H, $ArOCH_2$), 3.78 (s, 4H, OCH_2), 3.62 (s, 4H, OCH_2). Anal. calcd for $C_{33}H_{36}BF_4N_5O_5PdS_2$: C 40.03; H 3.73. Found: C 40.24; H 3.66.

[Pd(1)(guanine-BF_3)][BF_4] (15b): A solution of **3** (0.8 mL, 0.01 M) was sonicated for 15 min with a 10-fold excess of solid guanine and the mixture filtered. The solvent was evaporated and the resulting solid residue redissolved in a 1:1 solution of $CHCl_3$/MeCN. After approximately one week, several small crystals of the product were isolated and used in a single-crystal X-ray diffraction study. Not enough material was isolated to obtain reliable NMR spectra. Attempts to repeat this procedure to obtain more material for further spectroscopic analysis have not been successful to date.

[Pd(2)(guanine)][BF_4] (16): Compound **4** (25.0 mg, 0.034 mmol) and guanine (5.2 mg, 0.034 mmol) were stirred in MeCN (5 mL) and CH_3OH (5 mL) for 24 h. The resulting precipitate was washed with diethyl ether (5 mL) and recrystallized from MeCN/diethyl ether. Yield 17.6 mg (62%). ^{1}H NMR ($CDCl_3$): δ = 11.13 (s, 1H, NH), 9.68 (s, 1H, NH), 7.50 (s, 1H, H8G), 7.19-6.84 (m, 3H, Pd–Ar; 8H, *m*-Ar), 5.29 (s, 2H, NH_2), 4.48 (s, 4H, Bz), 4.28 (s, 4H, Bz), 3.95 (s, 4H, $ArOCH_2$), 3.82 (s, 4H, OCH_2), 3.68 (s, 4H, OCH_2). Anal. calcd for $C_{33}H_{36}BF_4N_5O_5PdS_2$: C 40.03; H 3.73. Found: C 39.87; H 3.58.

X-ray structure analyses: Colorless crystals of **1** were grown by slow evaporation of a CH_2Cl_2 solution of the compound. Yellow to yellow-orange crystals of **3**, **5** and **7** were grown by vapour diffusion of diethyl ether into an acetonitrile solution of the complex. Orange crystals of **13** and **14** were obtained by vapour diffusion of diethyl ether into an acetonitrile solution of the complex. Orange-red crystals of **15b**·$CHCl_3$ were isolated by slow evaporation of a $CHCl_3$ solution of **15a** during an attempted recrystallization of that complex. Diffraction experiments were performed on a four-circle Rigaku AFC6S or AFC5R (**15b**·$CHCl_3$ only) diffractometer with graphite-monochromatized $Mo_{K\alpha}$ radiation. The unit cell constants and orientation matrices for data collection were obtained from 25 centred reflections ($15 < 2\theta < 35°$). Machine parameters, crystal data, and data collection parameters are summarized in Tables 2, 7 and S-1 (deposited at CCDC). The intensities of three standard reflections were recorded every 150 reflections and showed no statistically significant changes over the duration of the data collections. The intensity data were collected using the ω–2θ scan technique, in four shells ($2\theta < 30$, 40, 45, and 50°). Absorption coefficients were calculated and corrections applied to the data. The data were processed using the TEXSAN software[14] package running on an SGI Challenge XL computer. For **1**, the positions of the sulfur atoms were determined by direct methods from the E-map with highest figure-of-merit, while for the metal complexes the position of the palladium atom was determined by conventional Patterson methods. For each compound the remaining non-hydrogen atoms were located from a series of difference Fourier map calculations. Refinements were carried out by using full-matrix least-squares techniques on F by minimizing the function $\sum w(F_o - F_c)^2$, where $w = 1/\sigma^2(F_o)$ and F_o and F_c are the observed and calculated structure factors. Atomic scattering factors[15] and anomalous dispersion terms[16] were taken from the usual sources. In the final cycles of refinement, all non-H atoms were assigned anisotropic thermal parameters except for the carbon atoms in **7** and **15b**. Fixed H atom contributions were included with C–H distances of 0.95 Å and thermal parameters 1.2 times the isotropic thermal parameter of the bonded C atoms. These H atoms were not refined, but all values were updated as refinement continued. Details of the data collection are summarized in Tables 1 and 7, and selected bonding parameters are listed in Tables 2, 3, 5, 6, and 8–10.[17]

0947-6539/97/0308-1212 $ 17.50+.50/0 Chem. Eur. J. 1997, 3, No. 8

Acknowledgment: We thank the NSERC of Canada for financial support of this research and SLM is grateful for a NSERC postgraduate scholarship. Jeffrey R. Hall is thanked for his original synthesis of the diathiaether **9**.

Received: February 12, 1997 [F615]

[1] a) J. F. Stoddart, H. M. Colquhoun, *Angew. Chem. Int. Ed. Engl.* **1986**, *25*, 487; b) J. F. Stoddart, R. Zarzycki, in *Cation Binding by Macrocycles* (Ed.: G. W. Gokel, Y. Inoue), Marcel Dekker, New York, **1990**, pp. 631; c) S. J. Loeb, in *Comprehensive Supramolecular Chemistry, Vol. 1* (Ed.: G. W. Gokel), Pergamon, Oxford, **1996**, Chapt. 20, pp. 733.

[2] a) J. E. Kickham, S. J. Loeb, *J. Chem. Soc. Chem. Commun.* **1993**, 1848; b) J. E. Kickham, S. J. Loeb, *Inorg. Chem.* **1994**, *33*, 4351; c) J. E. Kickham, S. J. Loeb, *ibid.* **1995**, *34*, 5656. d) J. E. Kickham, S. J. Loeb, *Organometallics* **1995**, *14*, 3584.

[3] J. E. Kickham, S. J. Loeb, S. L. Murphy, *J. Am. Chem. Soc.* **1993**, *115*, 7031;

[4] a) M. Shionoya, E. Kimura, M. Shiro, *J. Am. Chem. Soc.* **1993**, *115*, 6730; b) M. Shionoya, T. Ikeda, E. Kimura, M. Shiro, *ibid.* **1994**, *116*, 3848.

[5] a) C. J. van Staveren, J. van Eerden, F. C. J. M. van Veggel, S. Harkema, D. N. Reinhoudt, *J. Am. Chem. Soc.* **1988**, *110*, 4994; b) M. T. Reetz, C. M. Niemeyer, M. Hermes, M. Goddard, *Angew. Chem. Int. Ed. Engl.* **1992**, *31*, 135; c) A. R. van Doorn, D. J. Rushton, W. F. van Staveren-Nijenhuis, W. Verboom, D. N. Reinhoudt, *Recl. Trav. Chim. Pays-Bas*, **1992**, *111*, 421.

[6] Y. Aoyama, A. Yamagishi, M. Asagawa, H. Toi, H. Ogoshi, *J. Am. Chem. Soc.* **1988**, *110*, 4076; b) T. Mizutani, T. Ema, T. Yoshida, Y. Kurado, H. Ogoshi, *Inorg. Chem.* **1993**, *32*, 2072. c) H. Chen, S. Ogo, R. H. Fish, *J. Am. Chem. Soc.* **1996**, *118*, 4993 and references therein.

[7] a) S. C. Zimmerman, W. Wu, Z. Zeng, *J. Am. Chem. Soc.* **1991**, *113*, 196 and references therein; b) T. Tjama, G. Deslongchamps, J. Rebek Jr., *ibid.* **1990**, *112*, 8408; c) K. S. Jeong, T. Tjivikua, A. Muehldorf, G. Deslongchamps, J. Rebek Jr., *ibid.* **1991**, *113*, 201; d) G. Deslongchamps, A. Galan, J. de Mendoza, J. Rebek Jr., *Angew. Chem. Int. Ed. Engl.* **1992**, *31*, 61 and references therein; e) C. E. Osterberg, C. E. A. M. Arif, T. G. Richmond, *J. Am. Chem. Soc.* **1988**, *110*, 6903; f) D. P. Smith, E. Baralt, E. B. Morales, M. M. Olmstead, M. F. Maestre, R. H. Fish, *ibid.* **1992**, *114*, 10647 and references therein; g) Z. W. Li, H. Taube, *Science*, **1992**, *256*, 210.

[8] D. Voet, J. G. Voet, *Biochemistry*, 2nd ed., Wiley, New York, **1995**, p. 868.

[9] a) J. Buter, R. M. Kellogg, *J. Org. Chem.* **1981**, 4481; b) J. Buter, R. M. Kellogg, *Org. Synth.* **1987**, *65*, 150.

[10] a) G. S. Hanan, J. E. Kickham, S. J. Loeb, *Organometallics*, **1992**, *11*, 3063; b) G. R. Giesbrecht, G. S. Hanan, J. E. Kickham, S. J. Loeb, *Inorg. Chem.* **1992**, *31*, 3286.

[11] *CRC Handbook of Nucleobase Complexes: Transition Metal Complexes of Naturally Occurring Nucleobases and Their Derivatives, Vol. I* (Ed.: J. R. Lusty), CRC Press, Boca Raton, FL, **1990**, pp. 9–99.

[12] C. Price, M. R. J. Elsegood, W. Clegg, A. Houlton, *J. Chem. Soc. Chem. Commun.* **1995**, 2165.

[13] a) G. R. Desiraju, In *Crystal Engineering: The Design of Organic Solids*, Materials Science Monographs: No. 54, Elsevier, **1989**, p 92; b) C. A. Hunter, J. K. Sanders, *J. Am. Chem. Soc.* **1990**, *112*, 5525; c) S. K. Burley, G. A. Petsko, *ibid.* **1986**, *108*, 7995.

[14] TEXSAN-TEXRAY Structure Analysis Package, Molecular Structure Corp. (1985).

[15] D. T. Cromer, J. T. Waber, *International Tables for X-ray Crystallography*, Kynoch Press, Birmingham, **1974**, Vol. IV, Table 2.2A.

[16] a) J. A. Ibers, H. A. Hamilton, *Acta Crystallogr.* **1974**, *17*, 781; b) D. T. Cromer, *International Tables for X-ray Crystallography*, Kynoch Press, Birmingham, **1974**, Vol. IV, Table 2.3.1.

[17] Crystallographic data (excluding structure factors) for the structures reported in this paper have been deposited with the Cambridge Crystallographic Data Centre as supplementary publication no. CCDC-100176. Copies of the data can be obtained free of charge on application to the The Director, CCDC, 12 Union Road, Cambridge, CB21EZ, UK (Fax: Int. code +(1223)336-033; e-mail: teched@chemcrys.cam.ac.uk).